DØ Note 6205
March 30, 2012
DØ internal document, not for public distribution Version 1.2

Search for CP Violation in Single Top Quark Production in 5.4 fb^{-1} of Data

Suman Bala,[6] Victor Bazterra,[3] Aran Garcia-Bellido,[7] Jim Cochran,[4] Weigang Geng,[5] Cecilia Gerber,[3] Ann Heinson,[2] Shabnam Jabeen,[1] Jyoti Joshi,[6] Liang Li,[2] Mark Padilla,[2] Reinhard Schwienhorst,[5] Yun-Tse Tsai,[7] Nathan Triplett,[4] Steve Wimpenny.[2]

[1] *Brown University*
[2] *University of California, Riverside*
[3] *University of Illinois, Chicago*
[4] *Iowa State University*
[5] *Michigan State University*
[6] *Panjab University*
[7] *University of Rochester*

We present the search for CP violation in single top quark production with the D0 experiment at the Tevatron Collider. CP violation in the top electroweak interaction results in different production cross sections for top and anti-top quarks, distinguished by the charge of the lepton resulting from the top quark decay. In addition to the overall single top production asymmetry measurment, the analysis is also done in each of the single top production modes, s-channel and t-channel.

Contents

1. INTRODUCTION

The violation of Charge Conjugation and Parity symmetry (CP) is of a great importance in particle physics because its origins are not fully understood. CP violation processes can exist within the Standard Model (SM) by a CP-violating phase in the Cabibbo-Kobayashi-Maskawa (CKM) matrix. However, it is estimated that the amount of CP-violation from SM is not enough to explain baryogenesis, suggesting the possibility that new physics is needed to account for all CP-violating processes [1].

CP violation is a very rare phenomena that was only confirmed recently in the decay of K_L-mesons [2]. However, the amount of CP violation observed on these systems can be accommodated within the SM. More interesting are systems involving B-mesons where the expected CP-violating effects within SM are much larger [3]. On the other hand, the SM predicts very low CP violation for top physics because of the Glashow-Iliopoulos-Maiani (GIM) mechanism, making any large CP-violation effect direct evidence of physics beyond the SM [1, 3].

In this note, we present a search of CP violation in single top quark production and decay using the D0 detector at the Fermilab Tevatron. We exploit that the Tevatron is a $p\bar{p}$ collider, meaning that the initial state is a CP eigenstate and therefore, any difference between cross section for $p\bar{p} \to tX$ and $p\bar{p} \to \bar{t}X$ is a clear indication of CP violation [3, 4].

The difference between the top and antitop production cross sections is expressed through the production asymmetry:

$$\mathcal{A}_P = \frac{\sigma(p\bar{p} \to tX) - \sigma(p\bar{p} \to \bar{t}X)}{\sigma(p\bar{p} \to tX) + \sigma(p\bar{p} \to \bar{t}X)}. \tag{1}$$

However, since only the top quark decay products are observed in the detector, a possible asymmetry can also originate from the top quark decay $t \to bW^+$ or $\bar{t} \to \bar{b}W^-$, quantified by the partial rate asymmetry:

$$\mathcal{A}_D = \frac{\Gamma(t \to bW^+) - \Gamma(\bar{t} \to \bar{b}W^-)}{\Gamma(t \to bW^+) + \Gamma(\bar{t} \to \bar{b}W^-)} \tag{2}$$

Thus, the measured asymmetry $\mathcal{A}$ results from both production and decay contrubtions,

$$\mathcal{A} = \frac{\sigma(p\bar{p} \to tX)\mathcal{B}(t \to bW^+) - \sigma(p\bar{p} \to \bar{t}X)\mathcal{B}(\bar{t} \to \bar{b}W^-)}{\sigma(p\bar{p} \to tX)\mathcal{B}(t \to bW^+) + \sigma(p\bar{p} \to \bar{t}X)\mathcal{B}(\bar{t} \to \bar{b}W^-)}. \tag{3}$$

The decay asymmetry can be written as a function of $\Gamma(t \to bW^+) = \Gamma_t\mathcal{B}(t \to bW^+)$ and $\Gamma(\bar{t} \to \bar{b}W^-) = \Gamma_{\bar{t}}\mathcal{B}(\bar{t} \to \bar{b}W^-)$, where Γ_t and $\Gamma_{\bar{t}}$ are the total decay width for t and $\bar{t}$ quarks. Because of CPT conservation, $\Gamma_t = \Gamma_{\bar{t}} = \Gamma$ and the measured asymmetry can be expressed in terms of the partial decay rates,

$$\mathcal{A} = \frac{\sigma(p\bar{p} \to tX)\Gamma(t \to bW^+) - \sigma(p\bar{p} \to \bar{t}X)\Gamma(\bar{t} \to \bar{b}W^-)}{\sigma(p\bar{p} \to tX)\Gamma(t \to bW^+) + \sigma(p\bar{p} \to \bar{t}X)\Gamma(\bar{t} \to \bar{b}W^-)}\,. \tag{4}$$

which leads to a simplified relationship between production, decay and total asymmetry:

$$\mathcal{A} = \frac{\mathcal{A}_P + \mathcal{A}_D}{1 + \mathcal{A}_P\mathcal{A}_D}. \tag{5}$$

In this analysis we do not make any attempt to separate production from decay asymmetry and measure the total asymmetry $\mathcal{A}$.

We identify the production of single t or $\bar{t}$ quark using the charge of the lepton from the W boson decay from the top quark decay. We assume that no significant CP violation exists in the background samples. The analysis is done separately in the two single top quark production modes, t-channel and s-channel, which have different sensitivity to new physics [4, 5], and in the combined single top sample.

This analysis uses the same event selection,signal and background modeling, multivariate analysis techniques, statistical analysis methods and systematic uncertainties as the measurement of the single top quark production cross section using 5.4 fb^{-1} of DØ Run IIa and Run IIb data [7, 8]. The only updates are for the calculation of the asymmetry and two additional systematic uncertainties: A systematic uncertainty is added to account for the misidentification of the lepton charge, discussed in detail in Section 2. Another systematic uncertaintie is added to account for possible differences between b and $\bar{b}$ quarks, discussed in detail in Appendix 4. Section 3 gives the event yields separated by positive and negative lepton charge, Section 5 summarizes the systematic uncertainties, Section 6 describes how the asymmetry is measured and Sections 7 and 8 give the expected and observed results, respectively.

2. LEPTON CHARGE MIS-IDENTIFICATION

Charge measurement is important for this analysis since the CP violation can be dliluted by the mis-identification (mis-ID) of the lepton charge. We rely on the track charge to determine whether the selected lepton carries the positive or negative charge.

We select the $Z \to ee$ or $Z \to \mu\mu$ events to measure the charge mis-ID rate. We require each event to have exactly two electrons or two muons, and the invariant mass of the leptons between 80 and 100 GeV (Z peak). We assume all the same sign events (defined as the events containing two same sign leptons) under the Z peak must have one lepton with the wrong charge, and the opposite sign events (defined as the events containing two opposite sign leptons) have correctly measured lepton charges. Therefore the charge mis-ID rate is defined as the ratio between the number of same sign events and the total number of di-lepton events.

We measured the lepton charge mis-ID rate dependences on lepton detector eta and lepton transverse momentum using CSG 2EMhighpt and 2MUhighpt data samples. The luminosity of the data is 1.1 fb^{-1} for p17 and 4.3 fb^{-1} for p20.

We also measured the mis-ID rate from MC samples as a cross check.

Electron Channel data samples:

- CSG_CAF_2EMhighpt_PASS3_p18.13.01 for RunIIa
- CSG_CAF_2EMhighpt_PASS4_p21.10.00_p20.12.00 for RunIIb
- CSG_CAF_2EMhighpt_PASS4_p21.10.00_p20.12.01 for RunIIb
- CSG_CAF_2EMhighpt_PASS4_p21.10.00_p20.12.02 for RunIIb
- CSG_CAF_2EMhighpt_PASS4_p21.10.00_p20.12.05 for RunIIb
- CSG_CAF_2EMhighpt_PASS2_p21.10.00 for RunIIb

Electron Channel MC samples:

- AFB-Zee-60-130GeV-p21 for RunIIb
- AFB-Zee-60-130GeV-NoExtraSmear for RunIIa

Muon Channel data samples:

- CSG_CAF_2MUhighpt_PASS3_p18.14.00 for RunIIa
- CSG_CAF_2MUhighpt_PASS4_p21.10.00_p20.12.00 for RunIIb
- CSG_CAF_2MUhighpt_PASS4_p21.10.00_p20.12.01 for RunIIb
- CSG_CAF_2MUhighpt_PASS4_p21.10.00_p20.12.02 for RunIIb
- CSG_CAF_2MUhighpt_PASS4_p21.10.00_p20.12.03 for RunIIb
- CSG_CAF_2MUhighpt_PASS4_p21.10.00_p20.12.04 for RunIIb
- CSG_CAF_2MUhighpt_PASS4_p21.10.00_p20.12.05_summer2009 for RunIIb
- CSG_CAF_2MUhighpt_PASS2_p21.10.00 for RunIIb

Muon Channel MC samples:

- Zmumu-weigang-60-130GeV-p20_2 for RunIIb
- Zmumu-weigang-60-130GeV-p17 for RunIIa

For both channels we used the selection cuts as close as possible to the single top cross section measurement, except that we have 2 leptons instead of 1 (same isolation requirements for both leptons.), and we used the 2 jet inclusive bin while single top analysis uses 2, 3, 4 jet exclusive bins.

2.1. Electron Charge Mis-ID Rate

Electrons are defined as clusters of energy depositions in the electromagnetic section of the calorimeter, consistent in shape with an electromagnetic shower. We used these cuts for electrons in the charge mis-ID measurement:

- We require invariant mass $80 < M_{12} < 100$ GeV
- We require electrons to be within the central calorimeter with $|\eta^{\rm det}| < 1.1$ (CC).
- electron transverse momentum $p_T > 15$ GeV
- $z(\text{track}, \text{primaryvertex}) < 1$ cm
- At lease 90% of the energy of the cluster must be contained in the electromagnetice section of the calorimeter. EMF$>$ 90%
- The isolation requirement is ISO$<$ 0.15
- EM-likelihood$>$ 0.85
- 7×7 H-matrix $\chi^2 < 50$ HMx7cut $= 50$.
- Track $p_T > 5$ GeV
- RDCA$<$ 2. (= no rdca requirement.)
- Track match changed from spatial match only to also EOP match included ($track\_match\_spatialchi2prob()$ => $track\_match\_chi2prob()$). This further lowers electron misid rate from 0.6 to 0.3 percent.

Figure 1 shows the electron charge mis-ID rate as a function of $\eta^{\rm det}$ for Run IIa (left) and Run IIb (right).

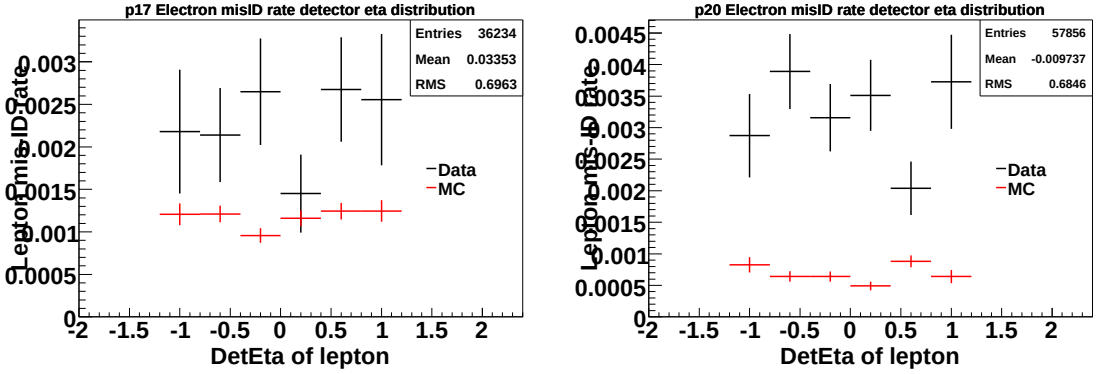

FIG. 1: The electron charge mis-ID rate as a function of $\eta^{\rm det}$ for Run IIa (left) and Run IIb (right).

Figure 2 shows the electron charge mis-ID rate as a function of lepton p_T for Run IIa (left) and Run IIb (right).

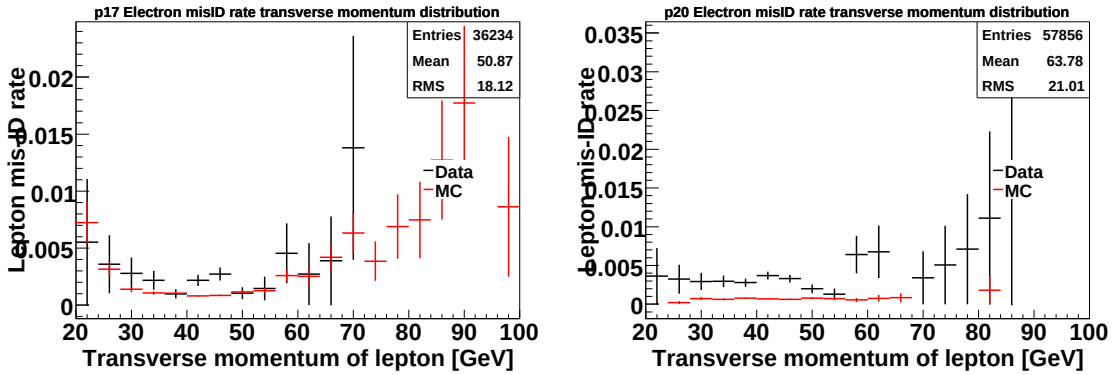

FIG. 2: The electron charge mis-ID rate as a function of lepton p_T for Run IIa (left) and Run IIb (right).

2.2. Muon Charge Mis-ID Rate

Muons are identified by combining tracks in the muon spectrometer ($\left|\eta^{\rm det}\right| < 2.0$) with central detectors tracks. We used these cuts for muons in the charge mis-ID measurement:

- We require Invariant Mass $80 < M_{12} < 100$ GeV
- We require muons to match the central calorimeter with $|\eta^{\rm det}| < 2.0$
- muon $p_T > 15$ GeV
- $z(\text{track}, \text{primaryvertex}) < 1$ cm
- We require muon not in a jet: $\Delta R(\text{muon}, \text{jet}) > 0.5$
- Momenta of all tracks are within $R < 0.5$ except muon track $< 20\%$ of muon pT: etTrkCone5/pT< 0.2
- energy in cone $0.1 < R < 0.4$ less than 20% of muon pT: etHalo/pT< 0.2
- pass 3 layers of muon scintilators: $|nseg| = 3$
- not from cosmic rays
- has a central track
- track $Chi2Ndf() < 4.0$
- when there is no SMT hits, require $DCA < 0.2$ (track match muon in η, ϕ.)

Figure 3 shows the muon charge mis-ID rate as a function of $\eta^{\rm det}$ for Run IIa (left) and Run IIb (right). We note that the shape of the data in eta is quite different from that of MC: the data seems to have a peak at 0. This is probably just fluctuation, the statistics are low and errors are big, e.g. p20 and p17 data "peak" at different positions. MC does not exhibit this behavior, only data.

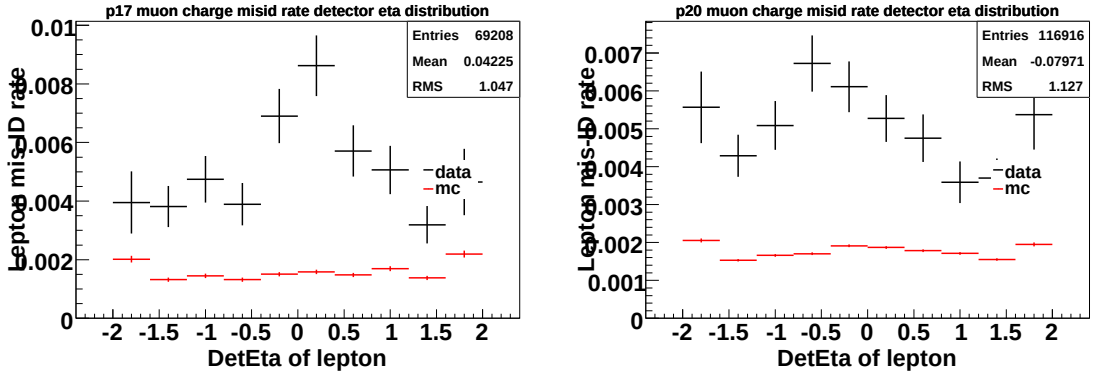

FIG. 3: The muon charge mis-ID rate as a function of $\eta^{\rm det}$ for Run IIa (left) and Run IIb (right).

Figure 4 shows the muon charge mis-ID rate as a function of lepton p_T for Run IIa (left) and Run IIb (right).

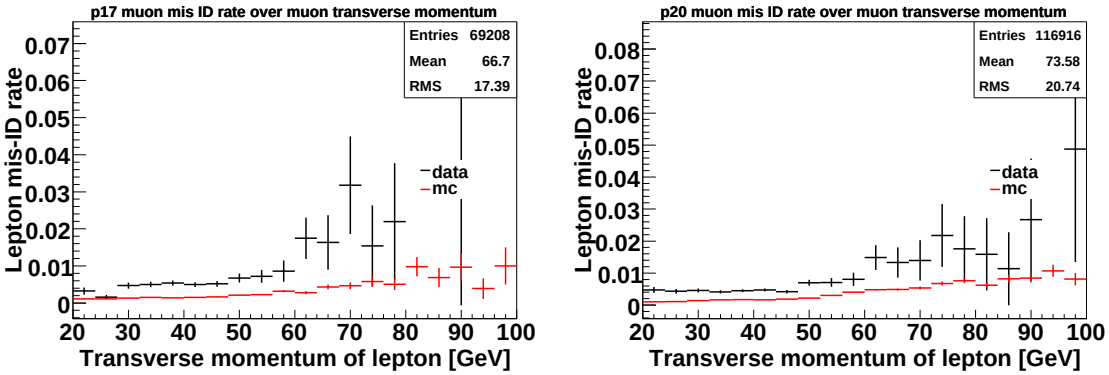

FIG. 4: The muon charge mis-ID rate as a function of lepton p_T for Run IIa (left) and Run IIb (right).

2.3. Charge mis-ID summary

In both MC and data, the fake rate is always below 1%. And since we are not sensitive to effects of the order of 1% compared to the existing much larger systematic uncertainites, we take this int account by adding a systematic uncertainty of 1%, anti-correlated between the positive and negative charge samples. One may note that the data charge mis-ID rate is higher than MC, though still less than 1%. The charge mis-ID rates, averaged over all η and p_T ranges, are shown in Table 1.

	Run IIa		Run IIb	
	Electron	Muon	Electron	Muon
Data	$0.22\%(1 \pm 0.11)$	$0.52\%(1 \pm 0.053)$	$0.32\%(1 \pm 0.074)$	$0.50\%(1 \pm 0.041)$
MC	$0.12\%(1 \pm 0.036)$	$0.15\%(1 \pm 0.016)$	$0.068\%(1 \pm 0.054)$	$0.18\%(1 \pm 0.0068)$

TABLE 1: Charge mis-ID rates summary.

3. EVENT SELECTION AND EVENT YIELDS

The event selection is described in detail in the selection note [7]. We split the samples by lepton charge, separating top and antitop quark production. The data-MC comparison plots after splitting are shown in Appendix 1. We use the same BNNComb discriminant as in Ref. [8]. The data MC comparison plots for BNNComb discriminants after splitting are shown in Appendix 2.

Tables 2 to 3 show the predicted and observed event yields for all signals and backgrounds after splitting the samples by lepton charge ("positive" and "negative" samples). Tables 4 to 5 show these yields for all signals and backgrounds before splitting [7].

The sum of the positive and negative yields is identical to the total as expected. The background normalization, in particular for W+jets and QCD multijets, is done before splitting and not done separately for positive and negative samples.

Note that the yield values shown in these and subsequent tables have been rounded for clarity, so that the sums of the components do not always equal exactly the values given for these sums, however all calculations have been done with full-precision values.

TABLE 2: Number of expected yields and observed data counts in "postive" samples after b-tagging.

Source	2 jets	3 jets	4 jets	All Channels
tb	53 ± 7.6	22 ± 3.7	6.4 ± 1.7	81 ± 13
tqb	70 ± 5.6	37 ± 4.4	13 ± 2.9	119 ± 13
tb+tqb	122 ± 13	59 ± 8.1	19 ± 4.6	200 ± 26
$t\bar{t}$	218 ± 41	418 ± 66	429 ± 77	1,066 ± 183
W+jets	1,773 ± 199	549 ± 67	149 ± 42	2,471 ± 307
Z+jets & dibosons	197 ± 28	73 ± 21	16 ± 9.0	286 ± 57
Multijets	133 ± 12	63 ± 5.8	21 ± 2.0	217 ± 20
Total prediction	2,443 ± 292	1,162 ± 166	635 ± 134	4,239 ± 592
Data	2,386 ± 49	1,161 ± 34	645 ± 25	4,192 ± 65
$S:B$	1:19	1:19	1:32	1:20

TABLE 3: Number of expected yields and observed data counts in "negative" samples after b-tagging.

Source	2 jets	3 jets	4 jets	All Channels
tb	52 ± 7.6	22 ± 3.7	6.5 ± 1.6	80 ± 13
tqb	71 ± 5.5	36 ± 4.2	13 ± 2.9	120 ± 13
tb+tqb	123 ± 13	58 ± 7.9	20 ± 4.5	200 ± 25
$t\bar{t}$	217 ± 42	415 ± 65	433 ± 78	1,065 ± 185
W+jets	1,789 ± 191	551 ± 86	135 ± 40	2,474 ± 316
Z+jets & dibosons	203 ± 29	68 ± 19	18 ± 9.6	289 ± 56
Multijets	144 ± 13	67 ± 6.2	22 ± 2.1	233 ± 21
Total prediction	2,475 ± 287	1,157 ± 183	628 ± 133	4,261 ± 603
Data	2,495 ± 50	1,146 ± 34	638 ± 25	4,279 ± 65
$S:B$	1:19	1:19	1:31	1:20

The observed counts in data agree with the prediction in the separate positive and negative samples, with variations as expected from statistical fluctuations.

Once tagged yields for combined signals and backgrounds								
	Electron+Muon, Run IIa+Run IIb							
	2 jets		3 jets		4 jets		All Channels	
Signals								
tb+tqb	198 ± 0.91		85 ± 0.63		26 ± 0.36		309 ± 1.2	
Backgrounds								
$t\bar{t}$	313 ± 1.8	(7.5%)	545 ± 2.8	(31%)	499 ± 2.8	(62%)	1,356 ± 4.4	(20%)
W+jets	3,222 ± 20	(78%)	961 ± 9.9	(55%)	239 ± 4.0	(30%)	4,421 ± 23	(66%)
Z+jets & dibosons	357 ± 6.8	(8.6%)	123 ± 4.3	(7.1%)	29 ± 1.7	(3.6%)	510 ± 8.2	(7.6%)
Multijets	258 ± 2.2	(6.2%)	117 ± 1.9	(6.7%)	37 ± 0.83	(4.6%)	412 ± 3.1	(6.1%)
Background Sum	4,150 ± 22		1,745 ± 11		804 ± 5.2		6,699 ± 25	
Backgrounds+Signals	4,348 ± 22		1,830 ± 11		830 ± 5.3		7,008 ± 25	
Data	4,284 ± 65		1,772 ± 42		851 ± 29		6,907 ± 83	
$S:B$	1:21		1:21		1:31		1:22	

TABLE 4: Once tagged event yields with statistical uncertainty for each jet multiplicity and for all analysis channels combined. The percentages are of the total background for each component.

Twice tagged yields for combined signals and backgrounds								
	Electron+Muon, Run IIa+Run IIb							
	2 jets		3 jets		4 jets		All Channels	
Signals								
tb+tqb	46 ± 0.37		31 ± 0.34		13 ± 0.22		90 ± 0.55	
Backgrounds								
$t\bar{t}$	121 ± 0.97	(23%)	285 ± 1.8	(63%)	361 ± 2.2	(86%)	767 ± 3.0	(55%)
W+jets	338 ± 5.1	(65%)	139 ± 3.2	(30%)	45 ± 1.7	(11%)	522 ± 6.3	(37%)
Z+jets & dibosons	42 ± 1.7	(8.1%)	18 ± 1.1	(4.0%)	5.9 ± 0.53	(1.4%)	66 ± 2.1	(4.8%)
Multijets	19 ± 0.62	(3.7%)	13 ± 0.64	(2.9%)	6.3 ± 0.33	(1.5%)	39 ± 0.95	(2.8%)
Background Sum	520 ± 5.5		456 ± 3.9		418 ± 2.8		1,394 ± 7.3	
Backgrounds+Signals	566 ± 5.5		487 ± 3.9		431 ± 2.8		1,484 ± 7.3	
Data	597 ± 24		535 ± 23		432 ± 21		1,564 ± 40	
$S:B$	1:11		1:15		1:33		1:16	

TABLE 5: Twice tagged event yields with statistical uncertainty for each jet multiplicity and for all analysis channels combined. The percentages are of the total background for each component.

4. MULTIVARIATE ANALYSIS

The single top analysis utilizes three multivariate techniques (BDT, boosted decision tree, NEAT, neuro-evolution of augmented technologies, and BNN, Bayesian neural network), which are then combined into one final filter using BNN. Such a BNN is trained separately in the s-channel analysis, the t-channel analysis, and for $s+t$ combined.

The existing combination BNN filter is used here, no separate training is done for positive and negative charge samples. However, since the MC statistics are reduced when separating into positive and negative charges, the binning transformation of the BNN output is repeated for the two separate samples. We apply a binning transformation to the BNN output to ensure that there is a minimum amount of effective background events in each bin. The procedure is described in detail in Appendix D of Ref. [9] and also used in the SM single top analysis [8].

Figure 49 shows the BNN combination discriminant for the s-channel, separated by lepton charge. The signal region is shown in Fig. 50. Figure 45 shows the BNN combination discriminant for the t-channel, separated by lepton charge. The signal region is shown in Fig. 46. Figure 41 shows the BNN combination discriminant for the t-channel, separated by lepton charge. The signal region is shown in Fig. 42.

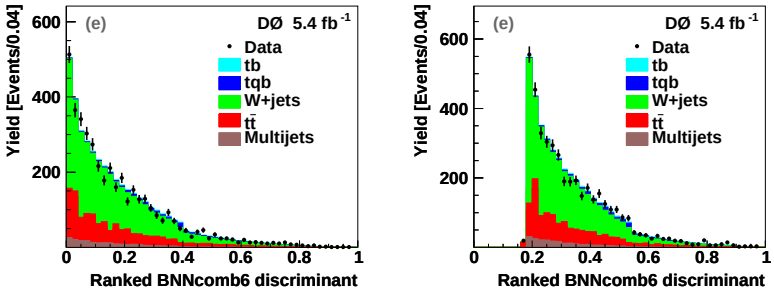

FIG. 5: The BNNcombSSort plots in the electron+muon channel for positive (left) and negative (right) events.

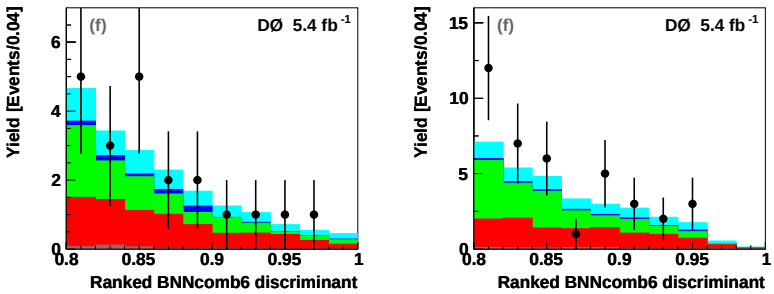

FIG. 6: The BNNcombSSortZoom plots in the electron+muon channel for positive (left) and negative (right) events.

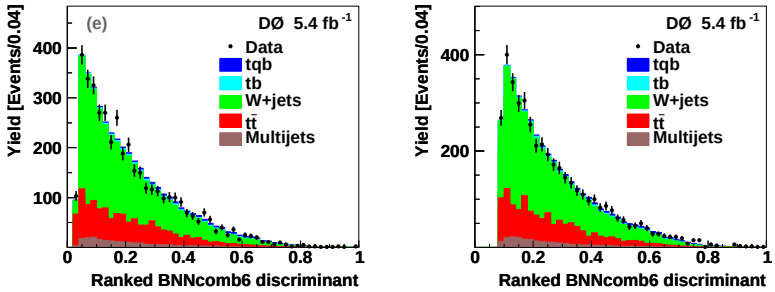

FIG. 7: The BNNcombTSort plots in the electron+muon channel for positive (left) and negative (right) events.

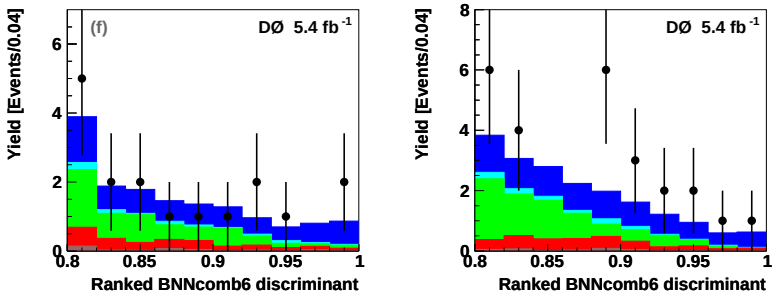

FIG. 8: The BNNcombTSortZoom plots in the electron+muon channel for positive (left) and negative (right) events.

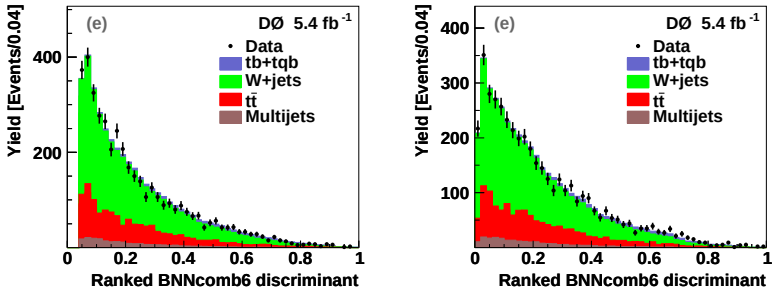

FIG. 9: The BNNcomb6Sort plots in the electron+muon channel for positive (left) and negative (right) events.

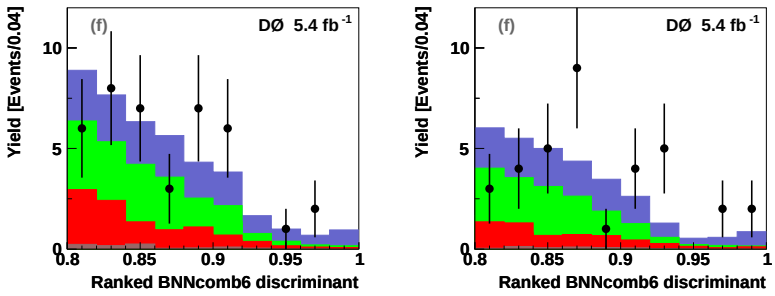

FIG. 10: The BNNcomb6SortZoom plots in the electron+muon channel for positive (left) and negative (right) events.

5. SYSTEMATIC UNCERTAINTIES

Systematic uncertainties for this analysis are the same as the selection note [7], except that two systematic uncertainties are added to account for lepton charge mis-identification and for jet-energy scale mis-modeling between b quarks and $\bar{b}$ quarks.

- **Integrated luminosity**
  The 6.1% uncertainty on the luminosity estimate affects the signal, $t\bar{t}$, Z+jets, and diboson yields.

- **Theory cross sections**
  The uncertainties on the single top and $t\bar{t}$ cross sections for 172.5 GeV are $\pm 3.8\%$ for s-channel tb, $\pm 5.3\%$ for t-channel tqb [14], and $+6.4\%, -9.0\%$ for $t\bar{t}$ [15]. The uncertainties on the Z+jets and diboson cross sections are 3.3% and 7%, respectively [16, 17].

- **Branching fractions**
  From the Particle Data Book, the branching fractions for a W boson to decay to an electron, muon, or tau lepton, have an average uncertainty of 1.5% and we include this in the MC normalization uncertainties.

- **Parton distribution functions**
  The effect of changing the parton distribution functions on the signals correspond to a systematic uncertainty of 2%. The PDF uncertainty on the $t\bar{t}$, Z+jets, and diboson background yields is included in the theory cross section uncertainties.

- **Trigger efficiency**
  We use an OR of many trigger conditions which give us a trigger efficiency of close to 100%, with an uncertainty of 5%, uncorrelated between p17 and p20 and between electrons and muons.

- **Instantaneous luminosity reweighting**
  The uncertainty on the modeling of the instantaneous luminosity is 1.0%.

- **Primary vertex modeling and selection**
  The uncertainty on the modeling and selection of the primary vertex is 1.4%.

- **Color Reconnection**
  The systematic on the modeling of color reconnection is 1.0% and is assigned as an additional uncertainty to the central efficiencies for $t\bar{t}$ background and signal MC.

- **Relative b/light jet response**
  The uncertainty in jet energy response between b quarks and light quarks is around 1% depending on the signal or background.

- **Electron reconstruction and identification efficiency**
  The electron modeling uncertainty is 2.8% for p17, and 3.8% for p20 data.

- **Muon reconstruction and identification efficiency**
  The muon modeling uncertainty is 2.1%.

- **Jet Fragmentation and higher-order effects**
  The uncertainty due to the jet fragmentation model and higher-order effects on the signal and $t\bar{t}$ samples is a few percent.

- **Initial-state and final-state radiation**
  The uncertainty due to ISR/FSR ranges from 0.8% to 10.9% and applies to signal and $t\bar{t}$ samples.

- **b-jet fragmentation**
  The uncertainty in the b-jet modeling is 2% and is applied to signal, $t\bar{t}$ and Zbb samples.

- **Taggability**
  The uncertainties associated with taggability of jets in MC events are between 3.1% and 21.5%.

- **W+jets heavy-flavor scale factor correction**
  The heavy-flavor scale factor uncertainty is 12%.

- **Z+jets heavy-flavor scale factor correction**
  The heavy-flavor scale factor uncertainty of 12% also applies to X+jets.

- **W+jets and multijets normalization**
  The uncertainty on the multijets background normalization is 30% (40% for the Run IIb MU channel). The uncertainty on the W+jets background normalizatioon is 1.8%.

- **Sample statistics**
  The limited MC event statistics uncertainty depend on the signal or background sample.

- **Jet reconstruction and identification**
  The efficiency to reconstruct and identify jets has an uncertainty varying from 0.04% to 3.7% for all MC samples. The effect of this uncertainty on the multivariate filter output is also taken into account.

- **Jet energy resolution**
  We assign a normalization and shape-changing uncertainty ranging from 0.2% to 11.6% as the jet energy resolution uncertainty for all signals and backgrounds.

- **Jet energy scale**
  The JES normalization uncertainty ranges from 0.3% to 14.6% for all MC samples. The effect of this uncertainty on the multivariate filter output is also taken into account.

- **Vertex confirmation**
  The efficiency to identify vertex-confirmed jets has an uncertainty varying from 0.1% to 9.6% for all MC samples. The effect of this uncertainty on the multivariate filter output is also taken into account.

- **b-tagging**
  The uncertainty associated with b-tagging in MC events ranges from 4.3% (5.8%) to 14.0% (11.2%) for single-tagged (double-tagged) samples. The effect of this uncertainty on the multivariate filter output is also taken into account.

- **V+jets angular corrections**
  The effect of the uncertainty due to the W and Z+jets background reweighting on the multivariate filter output is taken into account.

- **charge-mis ID**
  We assign a flat systematic uncertainty of 1% to account for differences between simulation and data as described in Section 2. This systematic uncertainty is anti-correlated between the postive and negative charge samples.

- $b/\bar{b}$ **JES**
  We assign a flat systematic uncertainty of 1% to account for possible differences in jet energy scale between b quarks and $\bar{b}$ quarks, as studied in Appendix 4.

A summary of the normalization components of the systematic uncertainties is given in table 6.

TABLE 6: A summary of the relative systematic uncertainties for each of the correction factors or normalizations. The uncertainty shown is the error on the correction or the efficiency, before it has been applied to the MC or data samples.

Relative Systematic Uncertainties	
Components for Normalization	
Integrated luminosity	6.1%
$t\bar{t}$ cross section	9.0%
Z+jets cross section	3.3%
Diboson cross sections	7.0%
Branching fractions	1.5%
Parton distribution functions	2.0%
(signal acceptances only)	
Triggers	5.0%
Instantaneous luminosity reweighting	1.0%
Primary vertex selection	1.4%
Color reconnection	1.0%
b/light jet response	(0.3-1.0)%
Electron identification	(2.8-3.8)%
Muon identification	2.1%
Jet fragmentation and higher order effects	(0.7-7.0)%
Initial-and final-state radiation	(0.8-10.9)%
b-jet fragmentation	2.0%
Taggability	(3.1-21.5)%
W+jets heavy-flavor correction	12.0%
Z+jets heavy-flavor correction	12.0%
W+jets normalization to data	1.8%
Multijets normalization to data	(30-40)%
MC and multijets statistics	(0.2-16)%
Charge-mis ID	1.0%
$b/\bar{b}$ jet energy scale	1.0%
Components for Normalization and Shape	
Jet reconstruction and identification	(0.04-3.7)%
Jet energy resolution	(0.2-11.6)%
Jet energy scale	(0.3-14.6)%
Vertex confirmation	(0.1-9.6)%
b tagging, single-tagged	(4.3-14.0)%
b tagging, double-tagged	(5.8-11.2)%
Angular correction	0.3%

6. EXTRACTING THE SINGLE TOP ASYMMETRY

The extraction of the cross sections tor top and antitop quark production is done using the samples separated by lepton charge. The likelihood is given by:

$$L(\mathbf{D}|\sigma_+,\sigma_-,\mathbf{a},\mathbf{b}) = \prod_{p=1} \frac{e^{-d_p} d_p^{D_p}}{\Gamma(D_p+1)} \prod_{n=1} \frac{e^{-d_n} d_n^{D_n}}{\Gamma(D_n+1)} \tag{6}$$

where $\mathbf{D}$, $\mathbf{a}$ and $\mathbf{b}$ are vectors of observed data, signal acceptance and background prediction. The cross sections for positive and negative leptons are given by $\sigma_+ = \sigma_t = \sigma(p\bar{p} \rightarrow tX)\mathcal{B}(t \rightarrow bW^+)$ for top quark production and $\sigma_- = \sigma_{\bar{t}} = \sigma(p\bar{p} \rightarrow tX)\mathcal{B}(\bar{t} \rightarrow \bar{b}W^-)$ for antitop quark production. The predicted number of events with positive and negative leptons are given by

$$\begin{aligned} d_p &= \sigma_+ a_p + b_p \\ d_n &= \sigma_- a_n + b_n. \end{aligned} \tag{7}$$

Here, a_p and a_n represent the single top acceptance times luminosity and b_p and b_n are the background yields for events with leptons with positive and negative charges. From this likelihood the following posterior probability density is defined:

$$p(\sigma_+,\sigma_-) = \frac{1}{\mathcal{N}} \int L(\mathbf{D}|\sigma_+,\sigma_-,\mathbf{a},\mathbf{b})\pi(\sigma_+,\sigma_-)\pi(\mathbf{a},\mathbf{b}) d\mathbf{a} d\mathbf{b}. \tag{8}$$

The asymmetry from Eq. 3 is thus written as

$$\mathcal{A} = \frac{\sigma_+ - \sigma_-}{\sigma_+ + \sigma_-} \;;\; \sigma = \sigma_+ + \sigma_- \tag{9}$$

where σ is the total cross section. Combining with Eq. 8, we obtain

$$p(\sigma,\mathcal{A}) = \frac{\sigma}{2\mathcal{N}} \int L(\mathbf{D}|\sigma(1+\mathcal{A})/2, \sigma(1-\mathcal{A})/2, \mathbf{a}, \mathbf{b})\pi(\sigma,\mathcal{A})\pi(\mathbf{a},\mathbf{b}) d\mathbf{a} d\mathbf{b}. \tag{10}$$

The prior is $\pi(\sigma,\mathcal{A}) = \pi(\sigma)\pi(\mathcal{A})$ where $\pi(\sigma)$ and $\pi(\mathcal{A})$ are flat priors in the interval $[0, \sigma_{\max}]$ and $[-1, 1]$, respectively. We then compute a posterior probability for the asymmetry $p(\mathcal{A})$ by integrating over the total cross section σ:

$$p(\mathcal{A}) = \int p(\sigma,\mathcal{A}) d\sigma \; . \tag{11}$$

7. EXPECTED RESULTS

The cross section is determined using the same Bayesian approach as in the cross section analyses using `top_statistics` [18]. The output of the combination discriminant, trained separately for single top s-channel (BNNCombS), t-channel (BNNCombT) and s+t-channel (BNNComb6) is used in the statistical analysis.

The asymmetry is measured from a 2d posterior that is a function of both the positive and the negative cross sections. This 2d posterior is constructed with no theoretical assumption on either the positive or negative cross sections. From this 2d posterior we extract the other measurement quantities: the asymmetry, the combined cross section, and the individual positive (negative) cross sections. Each of these is obtained by integrating over the 2d posterior to obtain a 1d posterior in the desired variable. The central value of the measurement is then taken from the peak in this 1d posterior density, and the 68% interval about the peak gives the uncertainty.

This procedure is done separately for $s+t$-channel (considering $s+t$-channel as signal and all other contributions as background), s-channel (considering s-channel as signal and adding the t-channel contribution to the backgrounds), and for t-channel (considering t-channel as signal and adding the s-channel contribution to the backgrounds). Figures 11 to 13 show the posterior density distributions.

All systematic uncertainties are included. The expected cross section is measured by setting the number of data events in each bin of each analysis channel to the expected number of background events plus the number of signal events predicted when using the SM cross section of 0.52 pb for s-channel, 1.13 pb for t-channel, and 1.65 pb for $s+t$-channel (for a top mass of 172.5 GeV).

The expected results for the CP asymmetry are shown in Table 7 for the case when no systematic uncertainties are included (nosys), when only normalization systematics are included (flat), and when all systematic uncertaintites are included (fullsys). The expected asymmetries are all very close to 0.

TABLE 7: Expected results for CP Asymmetry in s, t, s+t channels, with and without including systematic uncertainties.

Discriminant	Asymmetry	
	Statistical uncertainties only	Statistical and systematic uncertainties
tb	$-0.01^{+0.28}_{-0.30}$	$-0.04^{+0.28}_{-0.31}$
tqb	$-0.02^{+0.19}_{-0.20}$	$0.01^{+0.20}_{-0.19}$
tb+tqb	$-0.02^{+0.14}_{-0.14}$	$-0.01^{+0.14}_{-0.14}$

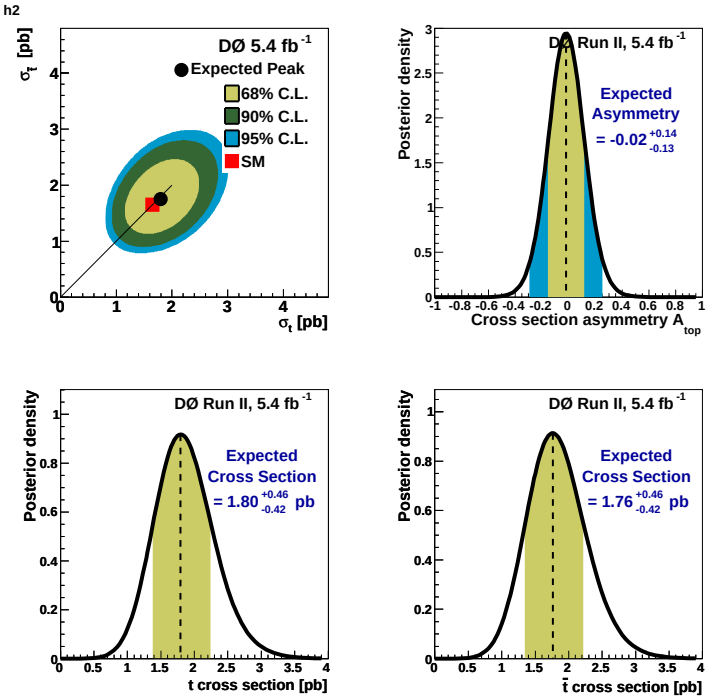

FIG. 11: Expected posterior density distributions and measurements of top and anti-top cross sections in the $s+t$-channel.

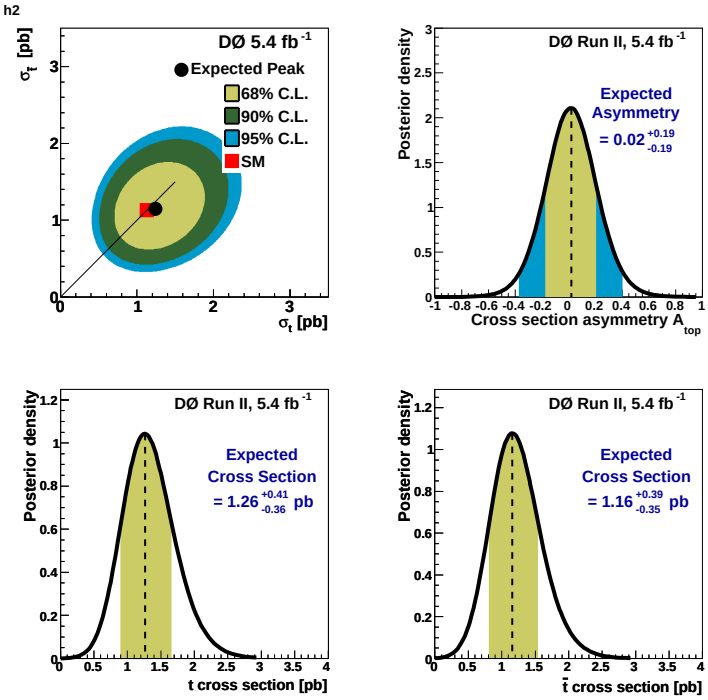

FIG. 12: Expected posterior density distributions and measurements of top and anti-top cross sections in the t-channel.

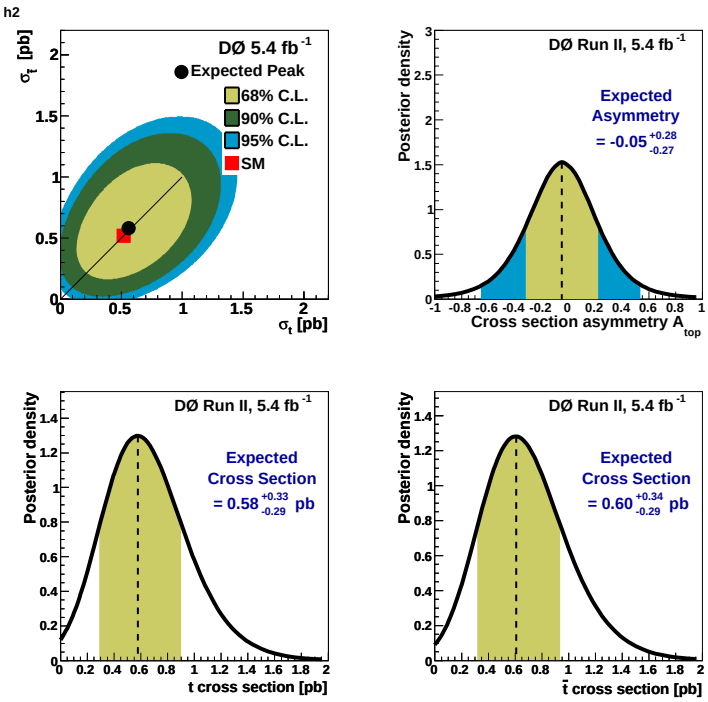

FIG. 13: Expected posterior density distributions and measurements of top and anti-top cross sections in the *s*-channel.

8. OBSERVED RESULTS

The observed asymmetry measurements are summarized in Table 8. The posterior density funcions are shown in Figs. 14 to 16, taking into account all systematic uncertainties.

TABLE 8: Observed CP Asymmetry in s, t, s+t channels including systematic uncertainties.

Discriminant	Asymmetry
tb	$-0.40^{+0.27}_{-0.33}$
tqb	$-0.22^{+0.16}_{-0.17}$
tb+tqb	$-0.21^{+0.14}_{-0.15}$

While the one σ contour overlaps with the SM expectation in each of the 2d posterior plots, the peak is away from the SM expectation of 0 more than one σ, though still less than two σ.

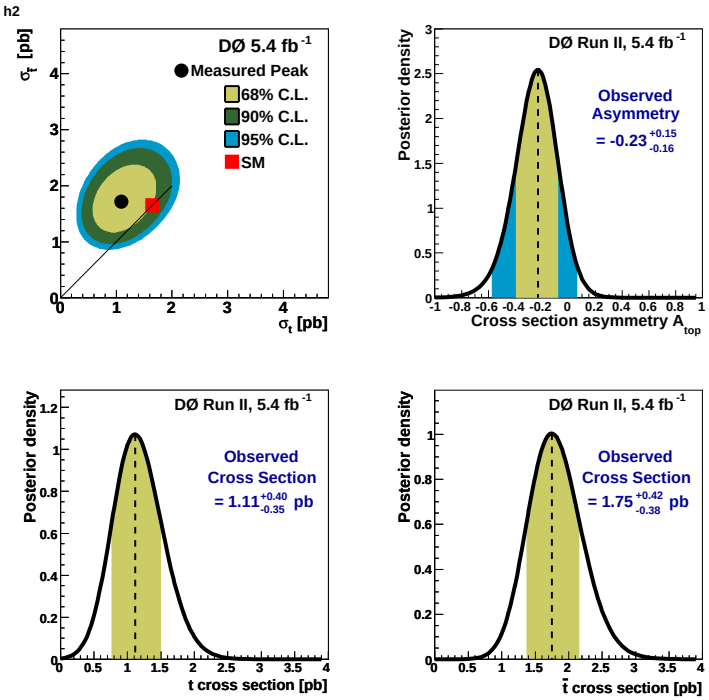

FIG. 14: Observed posterior density distributions and measurements of top and anti-top cross sections in the $s+t$-channel.

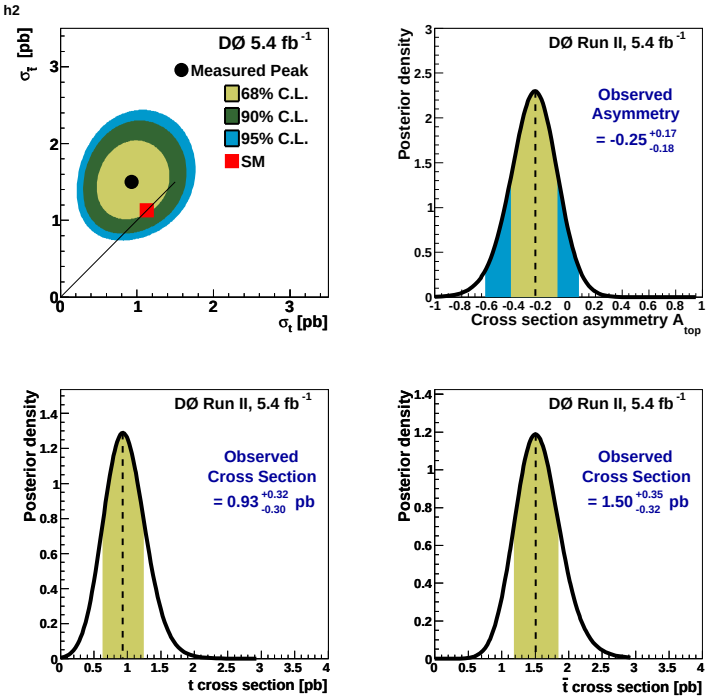

FIG. 15: Observed posterior density distributions and measurements of top and anti-top cross sections in the t-channel.

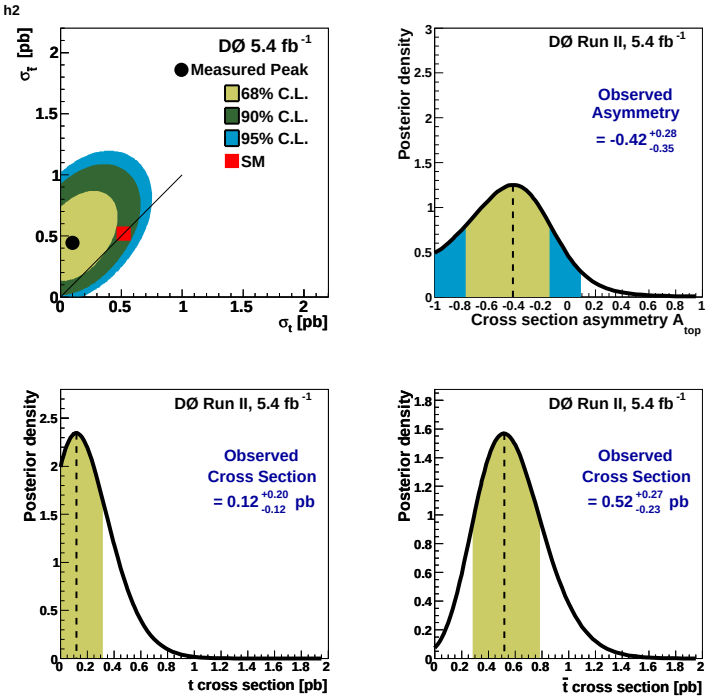

FIG. 16: Observed posterior density distributions and measurements of top and anti-top cross sections in the s-channel.

9. SUMMARY

In this note we present the search for CP violation using the single top quark final state with the D0 detector at the Fermilab Tevatron. We perform the search separately in the s-, t- and s+t-channel using 5.4 fb^{-1} of data. This analysis is an extension of the single top cross section measurement, and is the first analysis searching for CP voilation in single top quark production. The measured asymmetry $\mathcal{A}$ for s-, t- and s+t-channel are $-0.42^{+0.28}_{-0.35}$, $-0.25^{+0.17}_{-0.18}$ and $-0.23^{+0.15}_{-0.16}$ respectively.

APPENDIX 1 — PLOTS AFTER SPLITTING BY THE LEPTON CHARGE

Figures 17 to 39 show various kinematic distributions in the tagged final samples after being splitted by the lepton charge. The plots are shown as left for the positive samples and right for the negative samples.

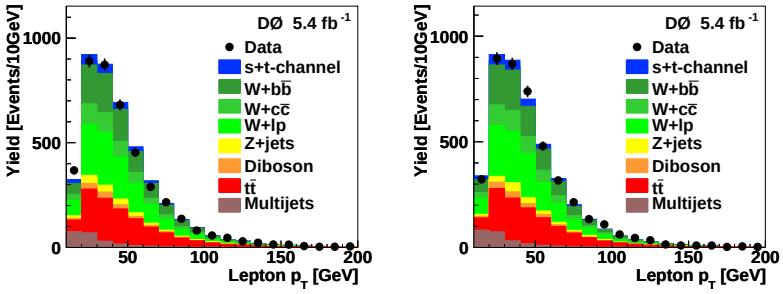

FIG. 17: The transverse momentum of the lepton in the electron+muon channel for positive (left) and negative (right) samples.

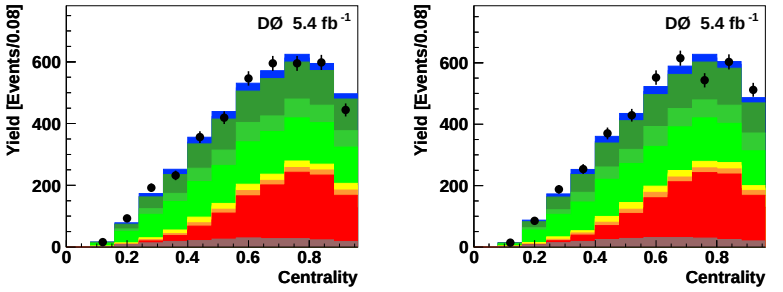

FIG. 18: The Centrality-AllJets in the electron+muon channel for positive (left) and negative (right) samples.

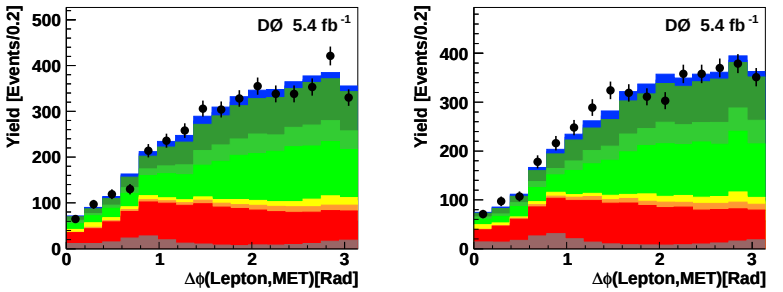

FIG. 19: The DeltaPhiLeptonMET in the electron+muon channel for positive (left) and negative (right) samples.

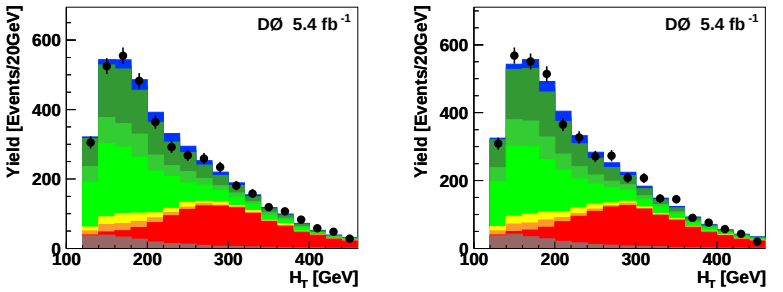

FIG. 20: The HT in the electron+muon channel for positive (left) and negative (right) samples.

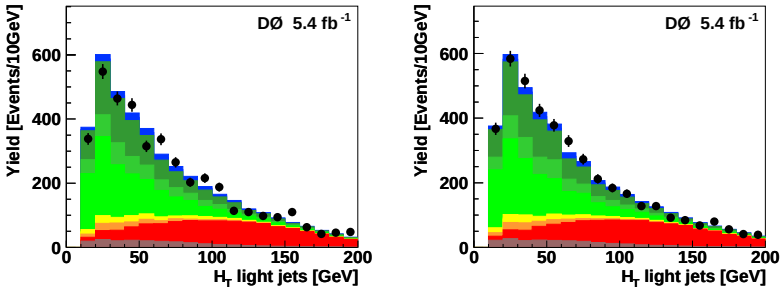

FIG. 21: The HT-AllJets-MinusBTaggedJet in the electron+muon channel for positive (left) and negative (right) samples.

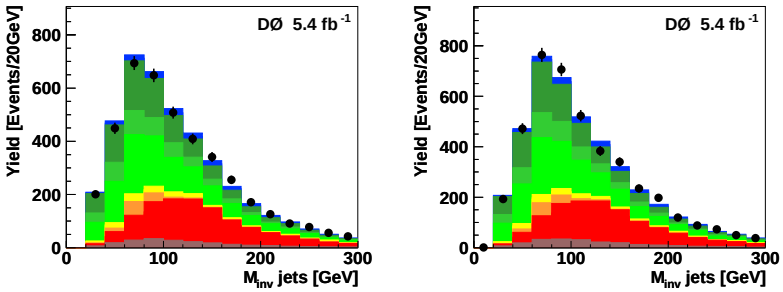

FIG. 22: The InvariantMass-Jet1Jet2 in the electron+muon channel for positive (left) and negative (right) samples.

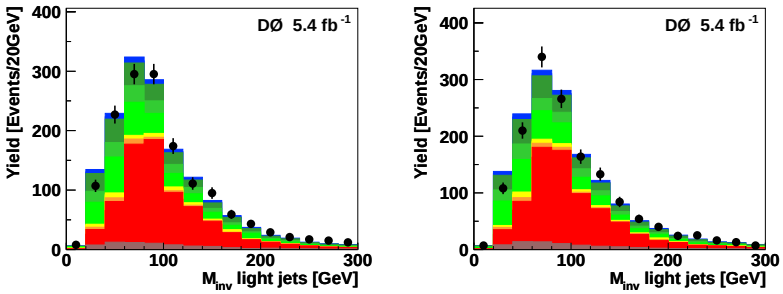

FIG. 23: The InvariantMass-LightQuarkJets1-2 in the electron+muon channel for positive (left) and negative (right) samples.

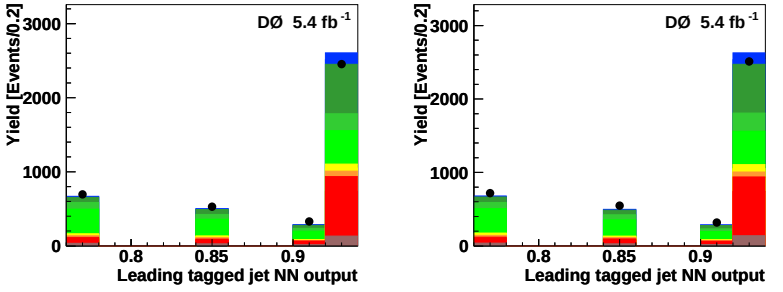

FIG. 24: The LeadingBTaggedJetBTagNN in the electron+muon channel for positive (left) and negative (right) samples.

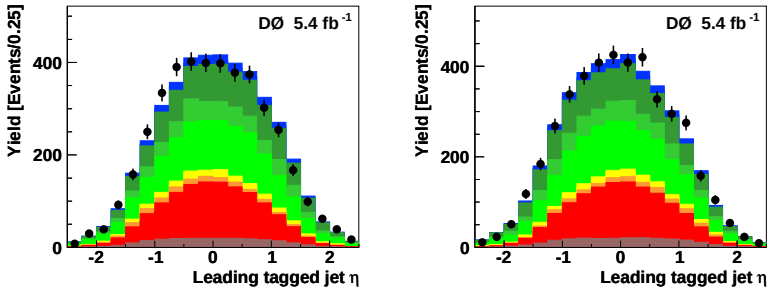

FIG. 25: The LeadingBTaggedJetEta in the electron+muon channel for positive (left) and negative (right) samples.

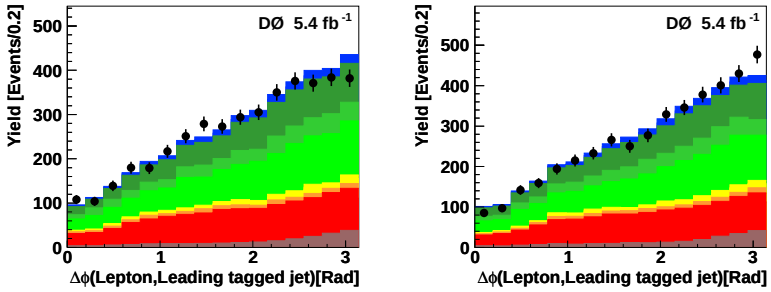

FIG. 26: The LeadingBTaggedJetLeptonDeltaPhi in the electron+muon channel for positive (left) and negative (right) samples.

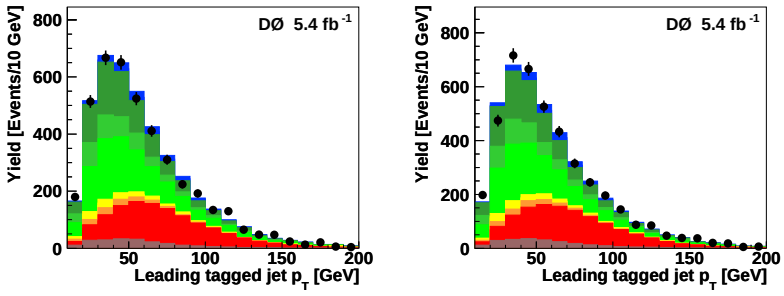

FIG. 27: The LeadingBTaggedJetPt in the electron+muon channel for positive (left) and negative (right) samples.

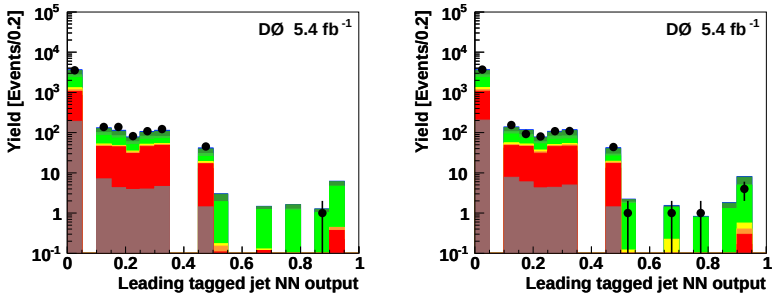

FIG. 28: The LeadingLightQuarkJetBTagNN in the electron+muon channel for positive (left) and negative (right) samples.

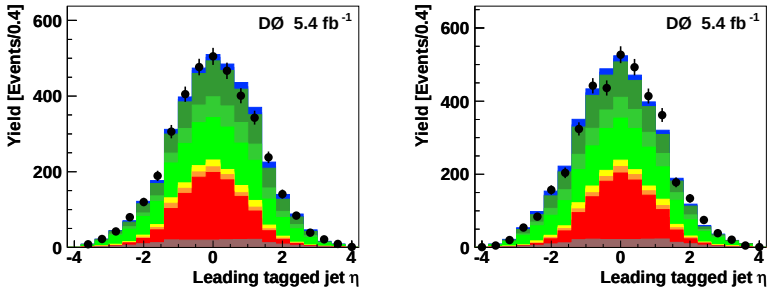

FIG. 29: The LeadingLightQuarkJetEta in the electron+muon channel for positive (left) and negative (right) samples.

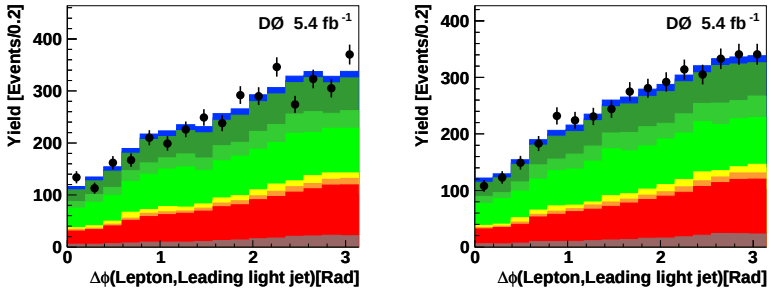

FIG. 30: The LeadingLightQuarkJetLeptonDeltaPhi in the electron+muon channel for positive (left) and negative (right) samples.

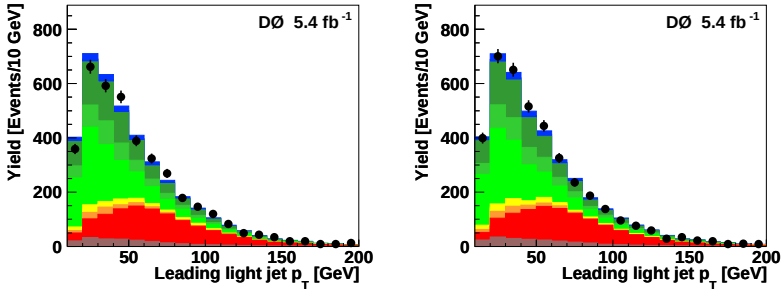

FIG. 31: The LeadingLightQuarkJetPt in the electron+muon channel for positive (left) and negative (right) samples.

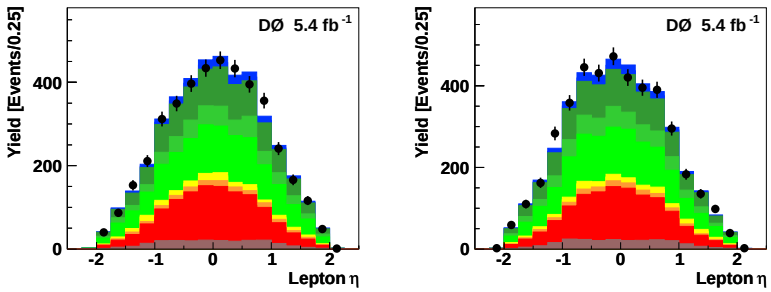

FIG. 32: The LeptonEta in the electron+muon channel for positive (left) and negative (right) samples.

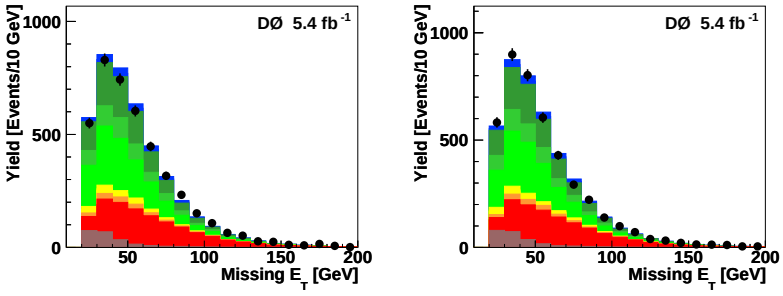

FIG. 33: The METPt in the electron+muon channel for positive (left) and negative (right) samples.

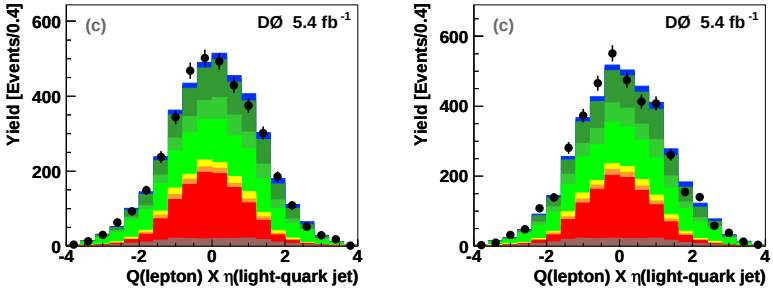

FIG. 34: The QTimesEta in the electron+muon channel for positive (left) and negative (right) samples.

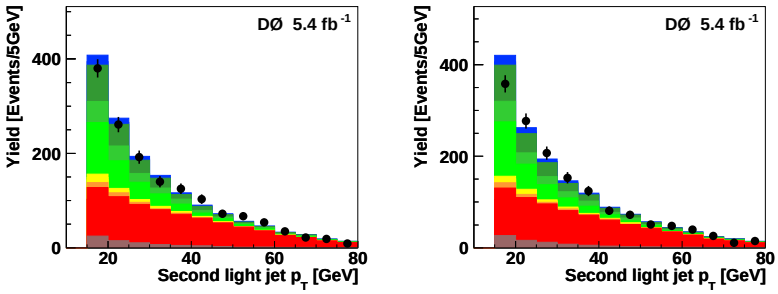

FIG. 35: The SecondLightQuarkJetPt in the electron+muon channel for positive (left) and negative (right) samples.

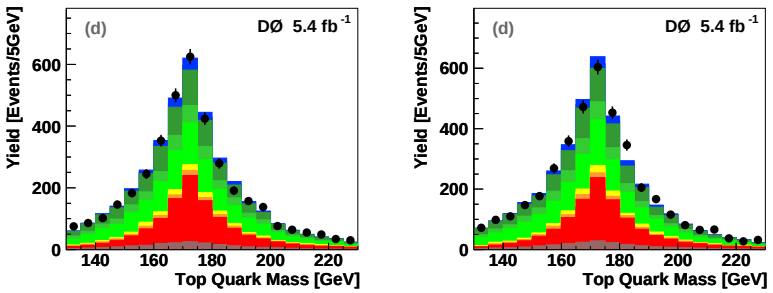

FIG. 36: The SigTopMass in the electron+muon channel for positive (left) and negative (right) samples.

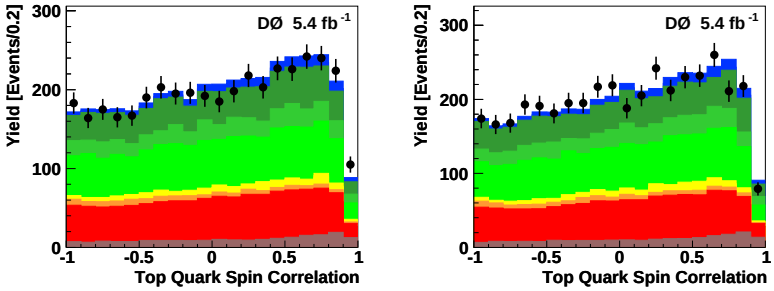

FIG. 37: The SpinCorr in the electron+muon channel for positive (left) and negative (right) samples.

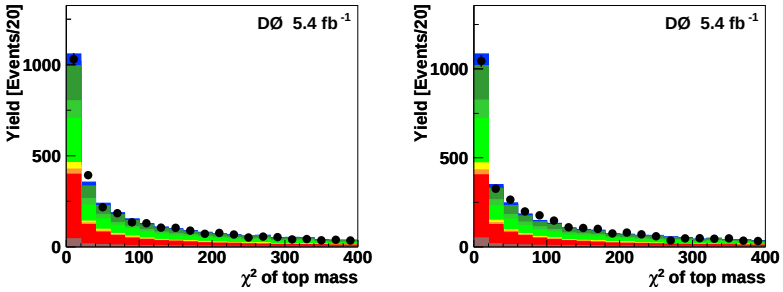

FIG. 38: The TopMassMinChiSqr in the electron+muon channel for positive (left) and negative (right) samples.

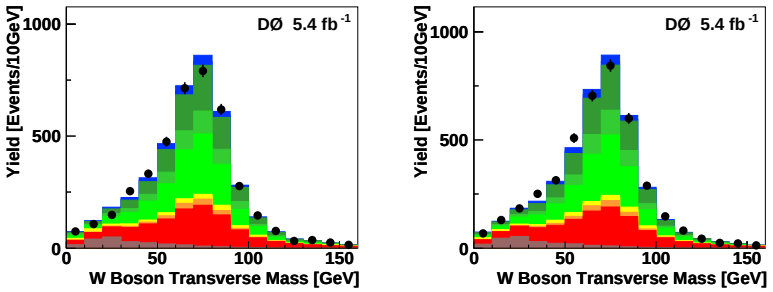

FIG. 39: The WT in the electron+muon channel for positive (left) and negative (right) samples.

APPENDIX 2 — PLOTS FOR DISCRIMINANTS AFTER THE BINNING TRANSFORMATION

Figures 40 to 51 show various discriminants distributions in the tagged final samples after the binning transformation applied to the discriminants [8, 9]. When trying to calculate the cross section, in the high discriminant region there may be some bins in which there are some signal but no background events. To avoid this, we applied a binning transformation to MVA outputs that ensures that there is a minimum amount of effective background events in each bin. We followed the same procedure as described in detail in Appendix D of Ref. [9] and applied the same binning transformation function derived for the BNNComb discriminants in Ref. [8] to both positive and negative charge samples.

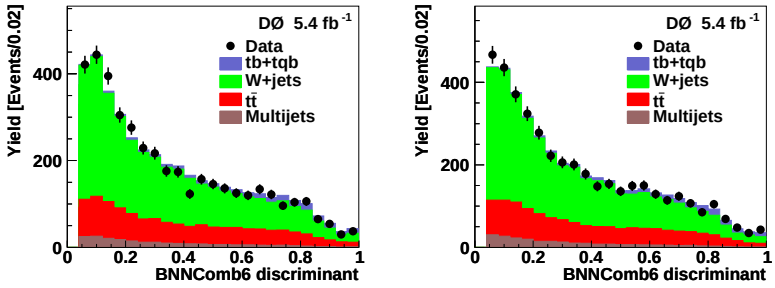

FIG. 40: The BNNcomb6 plots in the electron+muon channel for positive (left) and negative (right) events.

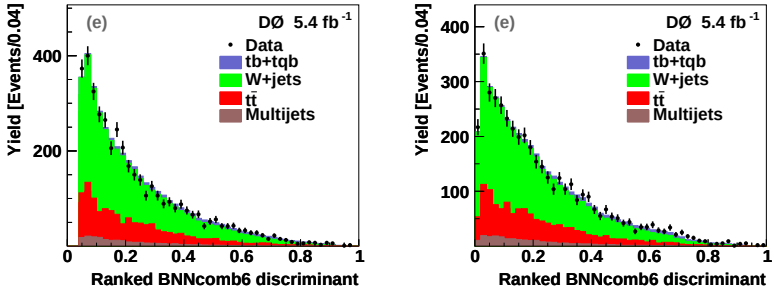

FIG. 41: The BNNcomb6Sort plots in the electron+muon channel for positive (left) and negative (right) events.

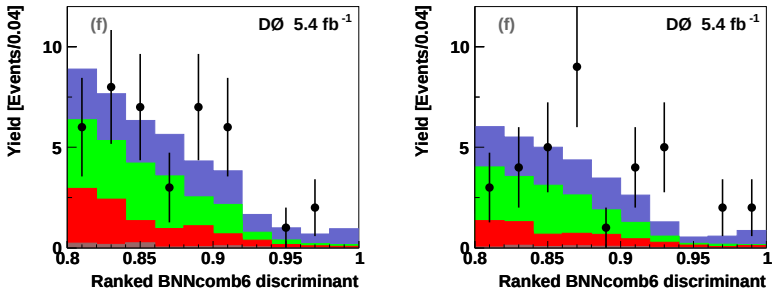

FIG. 42: The BNNcomb6SortZoom plots in the electron+muon channel for positive (left) and negative (right) events.

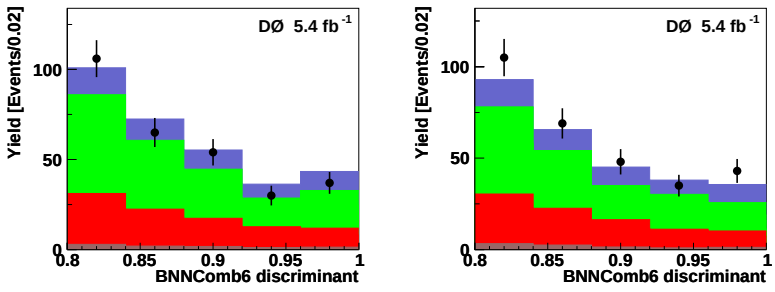

FIG. 43: The BNNcomb6Zoom plots in the electron+muon channel for positive (left) and negative (right) events.

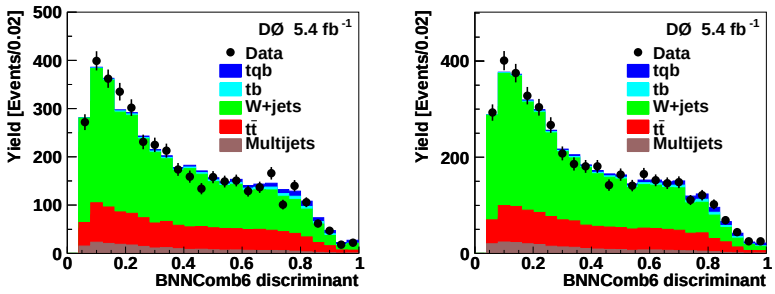

FIG. 44: The BNNcombT plots in the electron+muon channel for positive (left) and negative (right) events.

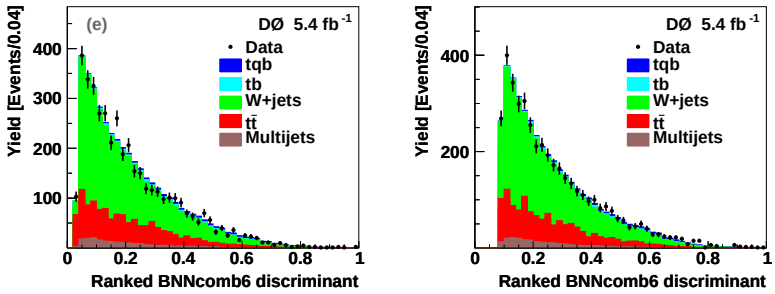

FIG. 45: The BNNcombTSort plots in the electron+muon channel for positive (left) and negative (right) events.

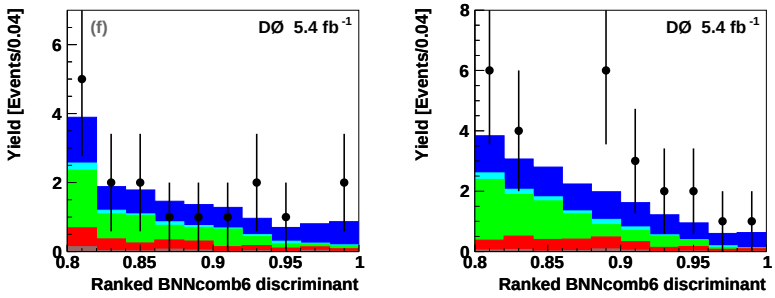

FIG. 46: The BNNcombTSortZoom plots in the electron+muon channel for positive (left) and negative (right) events.

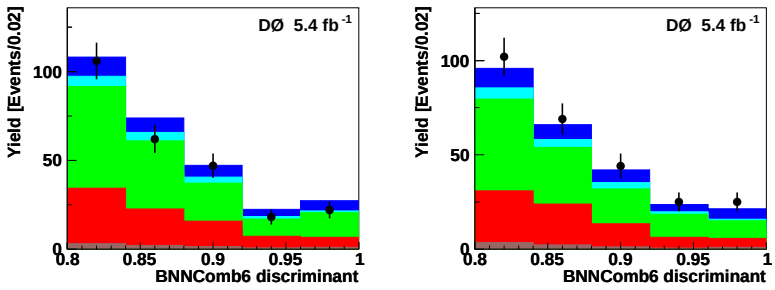

FIG. 47: The BNNcombTZoom plots in the electron+muon channel for positive (left) and negative (right) events.

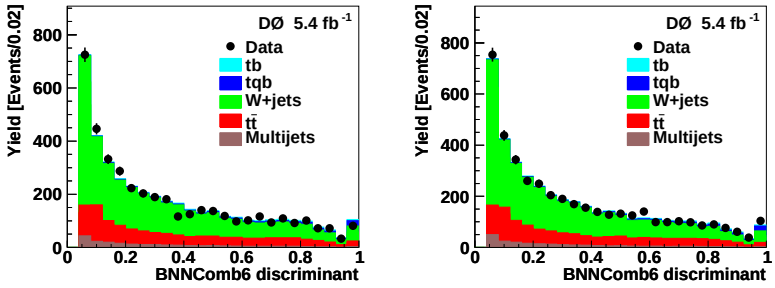

FIG. 48: The BNNcombS plots in the electron+muon channel for positive (left) and negative (right) events.

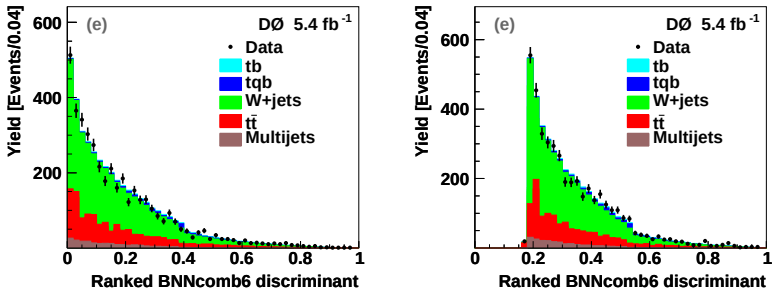

FIG. 49: The BNNcombSSort plots in the electron+muon channel for positive (left) and negative (right) events.

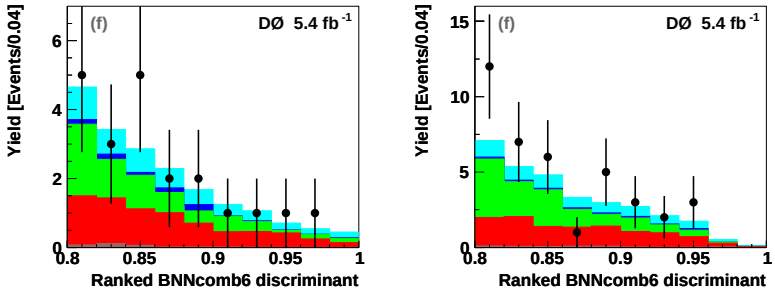

FIG. 50: The BNNcombSSortZoom plots in the electron+muon channel for positive (left) and negative (right) events.

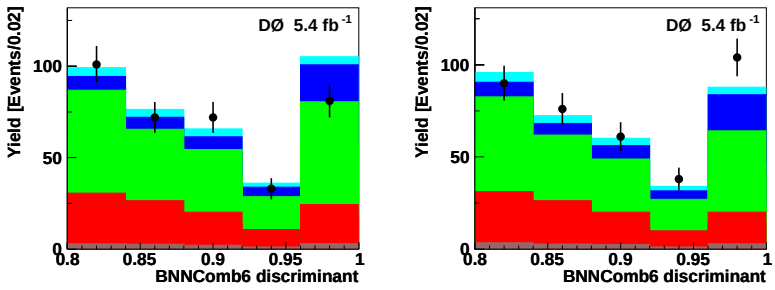

FIG. 51: The BNNcombSZoom plots in the electron+muon channel for positive (left) and negative (right) events.

APPENDIX 3 — W ASYMMETRY CHECK

We performed a systematic check for W^+ and W^- asymmetry using the W+jets sample. This check was done by using W+jets samples as the signal and *tbtqb* sample as a part of the backgrounds in the 2-jet and 1-tag bin. The expected and observed posterior density funcions are shown in Fig. 52 to Fig. 53 taking into account of all systematics. The W asymmetry is found to be consistent with 0 (as expected) and compared to the single top asymmetry we are trying to measure. This check excludes any possible bias from the detector effect.

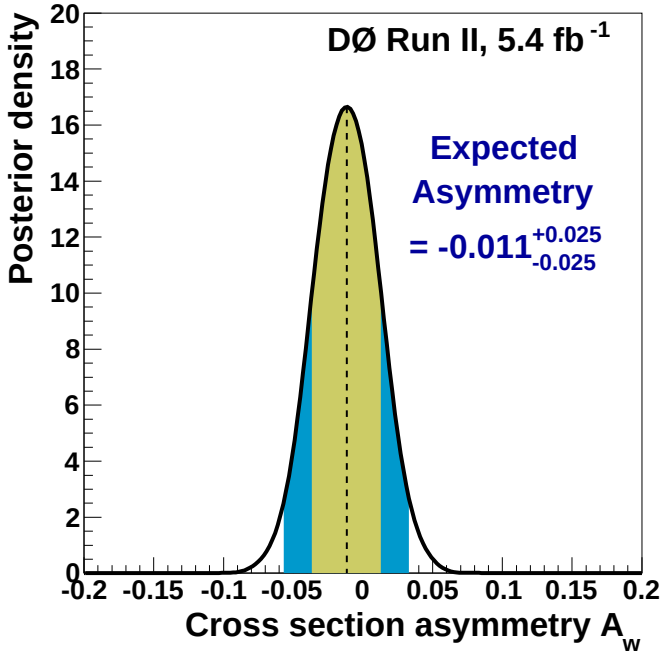

FIG. 52: Expected posterior density distributions for $W + jets$ asymmetry in the $s + t$-channel 2-jet 1-tag bin.

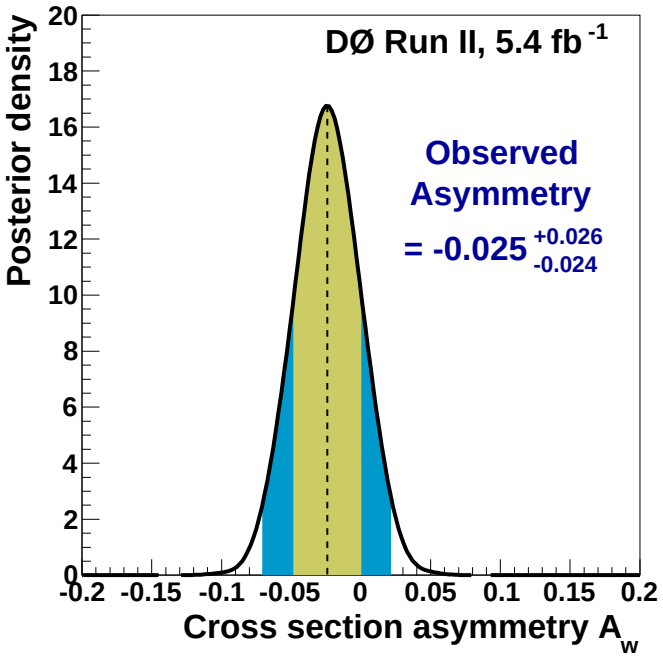

FIG. 53: Observed posterior density distributions for $W + jets$ asymmetry in the $s + t$-channel 2-jet 1-tag bin.

APPENDIX 4 — B/BBAR JES CHECK

The measurement of the top-antitop cross section difference could be affected by a different response of the calorimeter to quark and antiquark jets. Such a bias could come from a different calorimeter response to the b and the $\bar{b}$ decays, respectively. In principle, c and $\bar{c}$ responses in the calorimeter could affect $b/\bar{b}$ JES also, but it's an even smaller effect, so we did only b and $\bar{b}$ responses check only.

What we could do is to rescale the pT (the 4-vectors accordingly) of the b and $\bar{b}$ by a factor of 0.9971 and 1.0021 respectively [27], depending on b or $\bar{b}$, and then re-apply the MVA filters, for all MC samples. Then, we evaluate the difference in the CP violation extracted from the original and modified samples. However this would require "reweighting" the following samples: ttbar-lepjets,ttbar-dilepton,wbb,wcc,zbb,zcc,tb,tqb — this is almost the same amount of work compared to reskimming. Instead, we just do this for signal for check, which we expect will have the largest effect.

We expect the effect to be small as the measurement in top-antitop mass difference measurement. If this is the case, we would add another 1% flat systematic uncertainty.

Table 9 to 12 shows the expected event yields for signals after b-tagging before and after applying b/bbar JES for both "positive" and "negative" samples. We can see within errors the event yields did not change.

TABLE 9: Number of expected yields for signals in "postive" samples after b-tagging.

Source	2 jets	3 jets	4 jets	All Channels
tb	53 ± 7.6	22 ± 3.7	6.4 ± 1.7	81 ± 13
tqb	70 ± 5.6	37 ± 4.4	13 ± 2.9	119 ± 13
tb+tqb	122 ± 13	59 ± 8.1	19 ± 4.6	200 ± 26

TABLE 10: Number of expected yields for signals in "postive" samples after b-tagging for b/bbar JES.

Source	2 jets	3 jets	4 jets	All Channels
tb	53 ± 0.84	22 ± 0.54	6.5 ± 0.26	81 ± 1.5
tqb	70 ± 1.2	36 ± 0.95	13 ± 0.53	120 ± 2.4
tb+tqb	123 ± 1.9	58 ± 1.4	19 ± 0.74	200 ± 3.9

TABLE 11: Number of expected yields for signals in "negative" samples after b-tagging.

Source	2 jets	3 jets	4 jets	All Channels
tb	52 ± 7.6	22 ± 3.7	6.5 ± 1.6	80 ± 13
tqb	71 ± 5.5	36 ± 4.2	13 ± 2.9	120 ± 13
tb+tqb	123 ± 13	58 ± 7.9	20 ± 4.5	200 ± 25

TABLE 12: Number of expected yields for signals in "negative" samples after b-tagging for b/bbar JES

Source	2 jets	3 jets	4 jets	All Channels
tb	52 ± 0.84	22 ± 0.54	6.4 ± 0.26	80 ± 1.5
tqb	71 ± 1.2	36 ± 0.94	13 ± 0.52	120 ± 2.4
tb+tqb	123 ± 1.9	58 ± 1.4	19 ± 0.73	200 ± 3.9

[1] D. Atwood, S. Bar-Shalom, G. Eilan, A. Soni, "CP nonconservation in $p\bar{p} \to tbX$ at the Fermilab Tevatron", Phys. Rev. D **54**, 5412 (1996)

[2] J. Christenson, J.W. Cronin, V.L. Fitch and R. Turlay, "Evidence for the 2π Decay of the K20 Meson", Phys. Rev. Lett. 13, 138 (1964).

[3] D. Atwood, S. Bar-Shalom, G. Eilan, A. Soni, "CP Violation in Top Physics", Phys. Rept. 347, 1 (2001)

[4] C.-P. Yuan, "Strategies for Probing CP Properties in the Top Quark System at e^-e^+ and Hadron Colliders" Mod. Phys. Lett. A **10** 627 (1995)

[5] T. Tait and C.-P. Yuan, Phys. Rev. D **63**, 014018 (2000).

[6] The Single Top Working Group, "Single Top Quark Production in 2.3 fb^{-1} of Data – Signal and Background Modeling and Event Selection," DØ Note 5810, (2009).

[7] The Single Top Working Group, "Single Top Quark Production in 5.4 fb^{-1} of Data – Signal and Background Modeling and Event Selection," DØ Note 6099, (2010).

[8] The Single Top Working Group, "Measurement of the Single Top Quark Production Cross Section in 5.4 fb^{-1} of Data," DØ Note 6128, (2010)

[9] The Single Top Working Group, "Observation of Single Top Quark Production in 2.3 fb^{-1} of Data Using Boosted Decision Trees," DØ Note 5811, (2009).

[10] The Single Top Working Group, "Observation of Single Top Quark Production in 2.3 fb^{-1} of Data using Bayesian Neural Networks," DØ Note 5812, (2009).

[11] The Single Top Working Group, "Study of Single Top Quark Production in 2.3 fb^{-1} of Data using Matrix Elements," DØ Note 5813, (2009).

[12] The Single Top Working Group, "Combination of Three Single Top Quark Cross Section Measurements from 2.3 fb^{-1} of Data using a Bayesian Neural Network," DØ Note 5814, (2009).

[13] The Single Top Working Group, "Combination of Three Single Top Quark Cross Section Measurements from 2.3 fb^{-1} of Data using the BLUE method," DØ Note 5815, (2009).

[14] N. Kidonakis, Single Top Quark Production at the Fermilab Tevatron: Threshold Resummation and Finite-Order Soft Gluon Corrections," Phys. Rev. D **74**, 114012 (2006).

[15] Sven Moch and Peter Uwer, "Theoretical status and prospects for top-quark pair production at hadron colliders," Phys. Rev. D **78**, 034003 (2008).

[16] Frederic Deliot, Cecile Deterre, Slava Shary, "Z/$\gamma^\star$ cross section computation at NNLO using the FEWZ code," DØ Note 6050, (2010).

[17] Marc Buehler, Bob Hirosky, Shannon Zelitch (UVA) Gustaff Brooijmans, Lidija Zivkovic (Columbia U), "Search for standard-model Higgs production in the lepton + jets final state for $H- \to WW^* \to lnujj$ decay in 2.58 fb^{-1} of Run II Data," DØ Note 5851, (2009).

[18] S. Jain, H. Prosper and R. Schwienhorst, "Statistical Methods Implemented in the Package `top_statistics`," DØ Note 5817 (2008).

[19] The Single Top Working Group, "Measurement of $|V_tb|$ using the Single Top Quark Observation Analyses from 2.3 fb^{-1} of Data," DØ Note 5816, (2009).

[20] V.M. Abazov *et al.* (DØ Collaboration), "Observation of Single Top Quark Production," Phys. Rev. Lett. **103**, 092001(2009).

[21] V.M. Abazov *et al.* (DØ Collaboration), "Evidence for Production of Single Top Quarks and First Direct Measurement of $|V_{tb}|$," Phys. Rev. Lett. **98**, 181802 (2007).

[22] V.M. Abazov *et al.* (DØ Collaboration), "Evidence for Production of Single Top Quarks," Phys. Rev. D **78**, 012005 (2008).

[23] The Single Top Working Group, "Search for Single Top Quark Production in 1 fb^{-1} of Data," DØ Note 5285, (2007).

[24] L. Han, H. Yin, H. Schellman, J. Zhu, "Measurement of the Forward-Backward Charge Asymmetry (A_{FB}) in $p\bar{p} \to Z/\gamma^* \to e^+e^-$ events at $\sqrt{S} = 1.96$ TeV ," DØ Note 5867, (2010).

[25] S. Blessing, T. Hoang, "Measurement of the charge asymmetry in W to mu nu decay using the D0 detector ," DØ Note 5976, (2009).

[26] S. Bar-Shalom, D Atwood, and A. Soni, Phys. Rev. D **57**, 1495 (1998).

[27] O. Brandt et. al., "Measurement of the mass difference between top and antitop quarks in the lepton+jets channel using the matrix element method on 3.6 fb-1 of Run IIb data," DØ Note 6105, (2011).